

A Case Study of the Effect of the Observation Time in 3D-Var on Near-Surface Wind Forecasts in a Limited Region

Jianbo Yang¹, Min Shao^{2,3}, Qingeng Wang², and Xu Yang³

¹Tianjin Institute of Meteorological Science, Tianjin, China

²Atmospheric & Planetary Science, Hampton University, Hampton, VA, USA

³School of the Environment, Nanjing University, Nanjing, Jiangsu, China

Abstract

The relationships between the prediction of near-surface winds and the corresponding time of observations in eastern China were explored using the Advanced Weather Research and Forecasting (WRF) model and the three-dimensional variational (3D-Var) scheme in the gridpoint statistical interpolation (GSI) system. A series of one-month experiments was conducted in January 2018 with different time window configurations from 0.01 to 3.0 h. The relationship between the wind observation time and the model forecast was non-linear. An observational time closer to the initial time in the model usually have greater impact on the prediction of near-surface wind speeds. Observations in the 0.4–0.8 h time window associated with abnormally high with large near-surface wind speeds provide a negative impact. The predictions improved at a much smaller rate when the time window was increased from 0.8 to 3.0 h. No significant difference was seen as the time window increased in wind direction predictions, even with large wind increments. The optimum configuration of the time window in the GSI 3D-Var system for predicting near-surface winds should therefore be 0.2 or 0.4 h. A better understanding of the relationships between the observations and the predictions will help select more effective observations when using the 3D-Var scheme.

(Citation: Yang, J., M. Shao, Q. Wang, and X. Yang, 2019: A case study of the effect of the observation time in 3D-Var on near-surface wind forecasts in a limited region. *SOLA*, **15**, 172–177, doi:10.2151/sola.2019-031.)

1. Introduction

The accurate prediction of near-surface winds is a key problem in weather prediction systems. As a result of the complex interactions between the land surface and atmosphere within the planetary boundary layer (PBL), in addition to human impacts, near-surface winds are always more transient and intermittent than other atmospheric variables—for example, temperature and pressure show clear diurnal and seasonal variations (Belusic and Guttler 2010; Mahrt 2011; Zou et al. 2015). However, despite their transient and intermittent features, near-surface winds are an important factor in the lives of humans. Near-surface winds are affected by fluxes in momentum and wind shear in the PBL and have an important role in the transport and deposition of atmospheric pollutants, such as fine particulate matter, especially in urban areas (Yang et al. 2018). The accurate simulation/prediction of near-surface winds will not only improve our understanding of physical processes in the PBL, but will also provide reliable information for the simulation/prediction of atmospheric pollutants and the determination of their sources (Chen et al. 2015).

Because the development of physical processes and small- and meso-scale parameterization schemes in regional numerical weather prediction model is currently limited, especially for short-range forecasts, the accuracy of these systems has become more of an initial value problem (Zhang et al. 2015). Kalnay (2003) reported that an improved forecast can be obtained by initiating

the model with a better estimation of the initial conditions which served as the initial values for numerical models. Data assimilation is included in many numerical weather prediction systems as a key technique to improve the forecast. Assimilated observations from various sources can help to achieve a gridded estimation of the current atmosphere. Observations taken into the system through data assimilation affect the predictions at both observational and downstream regions (Lorenc 2003). For a specified data assimilation scheme, the performance is directly related to the quality and spatiotemporal distribution of the assimilated observations (Zhang et al. 2015). Global numerical weather prediction systems have been improved by the use of data from multiple satellites as a result of the large number and wide coverage of these observations (Baker et al. 2005; Xu et al. 2009).

The selection of wind observations is very important in the prediction of near-surface winds because such winds are strongly affected by terrain features, land surface processes, turbulence and the stability of the PBL. Although the assimilation of satellite observations can lead to better predictions of atmospheric profiles, many studies have shown that the assimilation of conventional observations alone can be more effective in the prediction of near-surface winds (Stauffer and Seaman 1991; Zapotocny et al. 2008; Cucurull and Anthes 2014; Zhang and Wang 2014; Zhang et al. 2015). The selection and configuration of data assimilation schemes will have a large impact on the prediction of near-surface winds. However, how the performance of near-surface wind predictions changes with the configuration of the data assimilation schemes and, more specifically, the width of time window, is still unclear. This study used the parameter “time window” to control the number of observations in the GSI system when only observations within the time window are retained for further assimilation analysis. The WRF model and the 3D-Var scheme in the GSI system were used to examine the relations among the configurations of data assimilation, the amount of data and the skill of the near-surface wind predictions.

This paper is organized as follows. Section 2 describes the model, data and experimental designs. The performance of near-surface wind predictions is analyzed in Sections 3 and 4 and the conclusions are provided in Section 5.

2. Model, data and experimental design

The Advanced Core of the Weather Research and Forecasting (WRF) model (Skamarock et al. 2008; Wang et al. 2011) is a non-hydrostatic, fully compressible, primitive equation model produced by the National Center for Atmospheric Research, the Air Force Weather Agency, the National Oceanic and Atmospheric Administration and other governmental agencies and universities. The physics schemes used in this study were as follows: the New Thompson scheme for microphysics (Thompson et al. 2008); the RRTMG schemes for both longwave and shortwave radiation (Iacono et al. 2008); the Mellor-Yamada Nakanishi and Niino (MYNN) surface layer scheme for surface layer (Nakanishi and Niino 2009); the RUC land surface model for surface physics (Benjamin et al. 2004); the MYNN Level 2.5 scheme for the planetary boundary layer (Nakanishi and Niino 2009); and the Grell-Freitas scheme for the cumulus parameterization (Grell and

Corresponding author: Min Shao, Hampton University, 100 E Queen St. Hampton, VA, USA. E-mail: mshao@masonlive.gmu.edu.



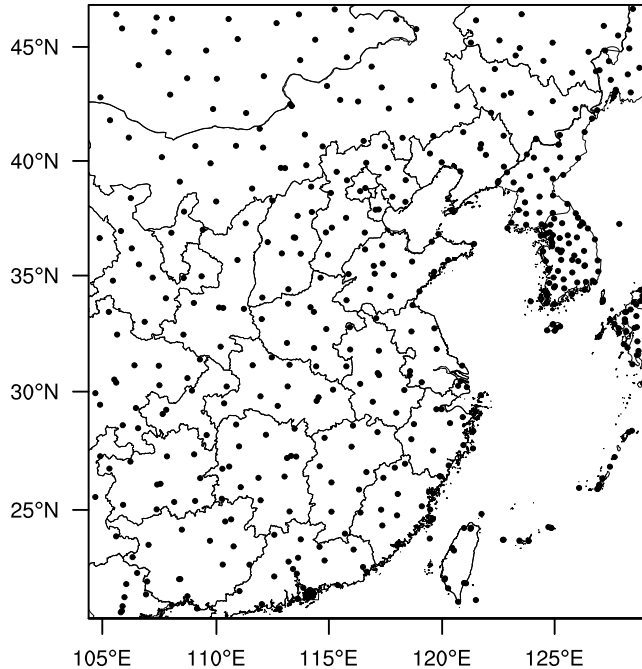


Fig. 1. Domain coverage showing the distribution of conventional observations (black dots).

Freitas 2014). The 3 h interval products from the Global Forecast System produced by the NCEP, which have a horizontal resolution of $0.5^\circ \times 0.5^\circ$ and 27 unevenly distributed vertical levels with a top at 10 hPa, were used as the initial atmospheric and lateral boundary conditions for the WRF-ARW model.

The WRF model was used to compare the performance of the near-surface wind predictions using different time windows in the GSI configuration. The model domain was designed with a horizontal grid spacing of $9\text{ km} \times 9\text{ km}$ to cover most of eastern China ($98.2^\circ\text{E}-135.2^\circ\text{E}, 20.5^\circ\text{N}-48.3^\circ\text{N}$) with 331×301 grid points. Figure 1 shows the model domain and coverage by conventional data (observations from > 300 stations). The climate of eastern China is mainly influenced by the East Asian monsoon, with a predominant northwest to southeast gradient in mean temperature and total annual precipitation (Chavas et al. 2009). A stronger East Asian monsoon and Siberian high were observed during the winter of 2017–2018, which resulted in a colder winter over eastern China with frequent cold front systems (Zhang and Song 2018).

The GSI (Kleist et al. 2009; Hu et al. 2016) system is a second-generation analysis system based on the operational Spectral Statistical Interpolation analysis system developed by the National Oceanic and Atmospheric Administration and the National Centers for Environmental Prediction (NCEP). The system is constructed in physical space and can be used for both global and regional applications. It is designed to be a flexible, state-of-the-art system that can be efficiently run on all parallel computing platforms. The GSI system can use all the observational data at the same time, including conventional observational data and satellite data. The types of conventional observations assimilated by the GSI include data from radiosondes, aircraft reports, surface land observations, surface ship and buoy observations, Doppler wind LiDAR and satellite retrievals.

The 3D-Var scheme in the GSI system was used in this study (Courtier et al. 1998; Rabier et al. 1998). Quality control steps were applied to the observations to avoid any data with large errors (Anderson and Jarvinen 1998). The GSI then read in all the data at the same time and minimized the cost function to obtain the optimized analysis through multiple iterations. The model state was first interpolated to the observational state and then the

innovation was calculated. 3D-Var uses much less computational resources than the Four-Dimensional Variational and the Kalman filter schemes without losing too much accuracy. Operational conventional observations constructed in Binary Universal Form for the Representation (BUFR) of meteorological data format and provided by the NCEP were used for both data assimilation and evaluation. The conventional observations included not only in-situ observations, but also some satellite retrievals, such as the Moderate Resolution Imaging Spectroradiometer infrared, water vapor and wind data. All the data can be downloaded at www.nco.ncep.noaa.gov/pmb/products/gfs/

Experiments with different time windows from 0.01 to 3.0 h (namely, T0.01, T0.05, T0.1, T0.2, T0.3, T0.4, T0.5, T0.6, T0.7, T0.8, T0.9, T1.0, T1.2, T1.4, T1.5, T2.0, T2.5 and T3.0) in the 3D-Var scheme were conducted from 1 January to 6 February 2018, representing a typical winter season. The default global background error covariance matrix (Kleist et al. 2009) was used to compare the effects of different time windows. The configurations were the same for all experiments, with the same observation forward operators, quality control decisions and two outer loops with 50 inner iteration steps. The scale factor for the vertical correlation lengths of the background error was set to 1. The scale factors for horizontal smoothing were set to 0.373, 0.746 and 1.5. Similar to the rapid refresh model, a 6 h cycling with parallel partial cycling was used in which large-scale information was reintroduced every 24 h from the Global Forecast System model (Benjamin et al. 2016; James and Benjamin 2017). All the available operational conventional observations were assimilated every 6 h and followed by a 24 h forecast. The near-surface wind predictions at 6 and 24 h forecast lead times were verified against the associated conventional observations.

3. Impact of different time windows on near-surface wind analysis

Table 1 shows the number of assimilated and rejected observations associated with the biases in different time windows in the GSI system. The major biases are from the velocity azimuth display next generation weather radar (NEXRAD) and pilot balloons (PB), whereas the scatterometer and surface marine observations (SMO) show smaller biases. Figure 2 plots the near-surface wind increments (Analysis with more data added minus background) of T0.01–initial, T0.5–0.4, T1.0–0.5 and T3.0–1.0 averaged during the experimental period. The shaded regions were significant at the 95% level (*t*-test). Figure 2a shows that most of the area reached the 95% significance level. Major changes to the initial near-surface wind field were located in continental China, Taiwan and the Korean peninsula because conventional observations are mostly located on land and data are very sparse over the oceans. The mean change in wind speed was about 1.03 m s^{-1} .

The near-surface increments in wind speed become more complex as the amount of assimilated observational data increased. In general, no significant difference was observed when the time window was increased from 0.01 to 0.4 h (data not shown). The mean change in wind speed was $< 0.03\text{ m s}^{-1}$ and the maximum change in wind speed was $< 0.4\text{ m s}^{-1}$. These changes are mainly due to the assimilation of scatterometer (average number of observations increased from 20 to 772). However, when the time window was increased from 0.4 to 0.5 h, the number of assimilated observations increased dramatically (Table 1; Fig. 3), which resulted in a clear change in the near-surface wind speed (Fig. 2b), reaching the 95% significance level with clear increases in wind speed in southeast China. The mean and maximum changes in wind speed were 0.27 and 1.70 m s^{-1} as the time window increased from 0.4 to 0.5 h, respectively. Between the time window 0.4 and 0.5 h, it is the rawinsondes followed by the scatterometer and surface marine observations that have obvious increase of assimilated observations. Among those three types of observations, it is the surface marine observations showed a negative impact on the initial bias. The number of assimilated observations continued to increase as the observational time window changed

Table 1. The number of assimilated/rejected data and bias in different types of observation in each time window.

Time window (h)	Assimilated/ rejected data	Observation type (bias/average number of assimilated data)*					
		Radinsondes	PB	NEXRAD	Wind Profiles	SMO	Scatterometer
0.01	4488/75	-1.78/3067	-2.44/7		-2.05/48	1.12/1347	1.16/20
0.4	5429/156	-1.79/3182	-2.45/7	-3.64/27	-2.05/49	1.20/1391	0.86/772
0.5	9762/186	-1.48/7249	-2.45/7	-3.73/28	-2.05/49	1.30/1402	0.70/1027
0.9	10906/301	-1.49/7312	-2.45/7	-3.81/54	-2.05/49	1.29/1412	0.68/2072
1.0	11781/354	-1.49/7312	-2.37/197	-3.86/54	-1.92/49	1.39/1855	0.69/2314
3.0	16353/622	-1.52/7386	-2.39/201	-3.96/166	-1.98/51	1.35/3118	0.70/5430

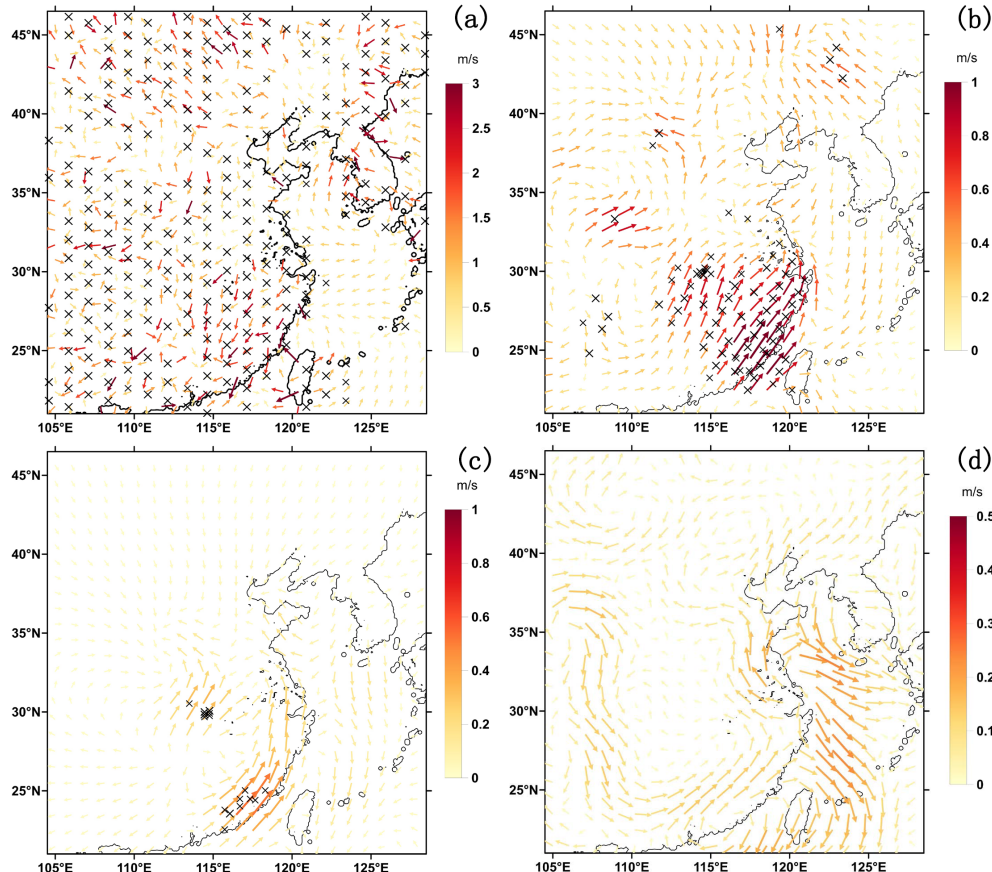


Fig. 2. Near-surface wind increments averaged from 6 January to 6 February 2018. (a) T0.01–initial, (b) T0.5–T0.4, (c) T1.0–T0.9 and (d) T3.0–T1.0. (The symbol of “x” denotes where the wind increments is statistically significant at the 95% confidence level.)

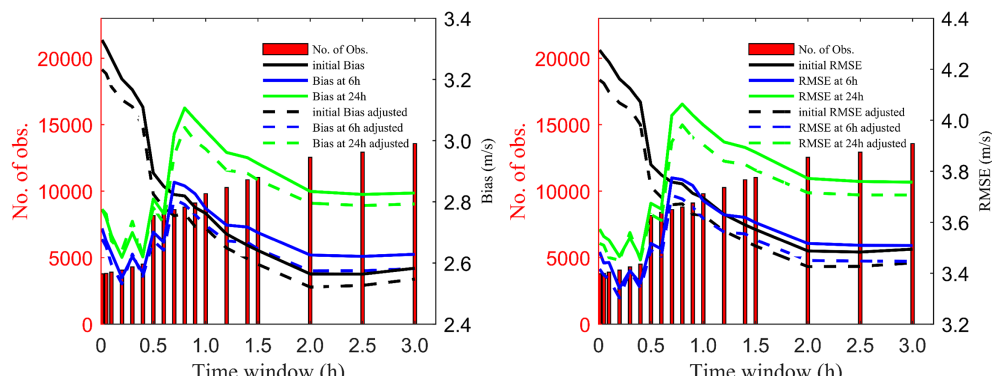


Fig. 3. Number of assimilated wind observations (red bars) and mean near-surface wind speed (a) bias and (b) RMSEs at the initial states (black solid lines) and at 6 h (blue solid lines) and 24 h (green solid lines) forecast lead times as a function of the time window, dashed lines are results with the anomalous events excluded.

from 0.5 to 0.9 h (Fig. 3), but the increases in the near-surface wind speed changed only slightly (maximum change in wind speed $< 0.1 \text{ m s}^{-1}$). At the window 0.5–0.9 h, only the number of assimilated scatterometer increased a lot, but the change of bias is relatively small which lead to small changes in near-surface wind speed bias and RMSE.

Figure 2c shows the changes in wind speed between the observation time windows of 0.9 and 1.0 h. The highest variations in the near-surface wind field were located in southeast China, with a strengthened southwesterly flow (maximum change in wind speed 0.55 m s^{-1}). However, only small regions reached the 95% significance level. No obvious modification of the near-surface wind field was observed for time windows $> 1.0 \text{ h}$. In Fig. 2d the mean change in wind speed was $< 0.1 \text{ m s}^{-1}$ and the maximum change was about 0.2 m s^{-1} .

These results show that the introduction of the GSI system can lead to a pronounced change in the initial near-surface wind field. The configuration of the observational time window in the GSI system was more sensitive when it was increased from 0.4 to 0.5 h and 0.9 to 1.0 h, although the modification of the near-surface wind is limited when time window increased above 1.0 h.

4. Effect of different time windows on the prediction of near-surface winds

The GSI system can assimilate all the observations within the time window at the same time. Therefore the model state was first interpolated to the observational state and then the innovation and cost function gradient were calculated. Ideally, for the assimilation of near-surface winds, better quality initials are obtained when the observational time is close to the analysis time and therefore the assimilation of a closer near-surface wind observation should lead to better predictions.

Figure 3 plots the number of assimilated wind observations and the mean absolute bias and root mean square error (RMSE) of the near-surface wind speed. The impact of using different time windows on the prediction of near-surface winds was more complex than expected. For the initial near-surface wind field shown in Figs. 3a and 3b (black lines), both the bias and RMSE were significantly reduced as the time window expanded from 0.01 to 2.0 h with more observations being assimilated (red bars). However, when the time window extended further from 2.0 to 3.0 h, there was no reduction in either the bias or RMSE.

Four stages were found in the variation trend of the predicted near-surface wind biases (RMSEs) as a function of the time window as it expanded from 0.01 to 0.4, 0.4 to 0.8, 0.8 to 2.0 and 2.0 to 3.0 h. Both the bias and the RMSE of the predicted near-surface wind fluctuated in an unstable manner for time windows in the range 0.01 to 0.4 h and reached a minimum value at 0.2 or 0.4 h. A noticeable increase in the bias and the RMSE was observed when the time window increased from 0.4 to 0.8 h. The forecast bias and RMSE then decreased for time windows from 0.8 to 2.0 h. When the time window of the GSI system was $> 2.0 \text{ h}$, it had little effect on the prediction of near-surface winds. The impacts on the 24 h forecast were similar to those on the 6 h forecast. Both the bias and RMSE had similar, but slightly larger, values in the 24 h forecast than in the 6 h forecast. However, when time window was $> 0.8 \text{ h}$, both the bias and RMSE increased much faster in the 24 h forecast than in the 6 h forecast. The absolute mean and standard deviation of the biases that dropped in the time window 0.4 and 1.0 h are 2.83 and 2.50 m s^{-1} , respectively. These numbers are larger than the absolute mean and standard deviation of the bias that dropped in the time window 0 and 3.0 h (2.58 and 2.35 m s^{-1} , respectively). Therefore observations with an observational time closer to the analysis time had larger impacts on predictions, whereas the observations with an observational time far away from the analysis state introduced more uncertainties during the steps of converting model state to “observed first guesses” via observational forward operator. The forecast bias and RMSE were at a minimum for time windows of 0.2 or 0.4 h and therefore should be selected as the optimum time window for the

prediction of near-surface winds.

Furthermore, the time-series of 6- and 24-h predicted near surface wind speed absolute biases (Figure not shown) show two periods (First period: 10–11 January; second period: 25–26 January) of large bias values existed in the experiment T0.8 compared to other experiments. The mean biases of 6-h predicted near surface wind speed that dropped in the time window 0.4–0.8 h and 0–3.0 h during the first period are -3.18 and 0.99 m s^{-1} , respectively. For the second period, the mean biases are 3.54 and 2.63 m s^{-1} , respectively. For the 24-h predictions, the biases differences between the time window 0.4–0.8 h and 0–3.0 h are even larger. The observations that bring large bias into the system during both periods are found to be NEXRAD at $(35.92^\circ\text{N}, 126.62^\circ\text{E})$ and $(26.31^\circ\text{N}, 127.9^\circ\text{E})$. In the first guess, the near surface wind speed mean biases in the two time windows (0.4–0.8 h and 0–3.0 h) are -1.74 , 0.29 and 2.13 , -0.11 m s^{-1} , for the two periods respectively. The initial sea level pressure (SLP) and 10 m height wind vectors anomaly are calculated using the differences between the period with large biases and the average state of the whole experimental period (Fig. 4). As shown in Fig. 4, large biases existed over the southeast ocean area in both periods. During the first period, an abnormally high was developed over the northeast of mainland China with wind speed difference exceeded 10 m s^{-1} where another large biases region was found. During the second period, it was an abnormally low in the north but abnormally high in the south of mainland China. Both periods showed low system at the northeast of China at 500 hPa level and strong cyclones at 850 hPa. The region with large biases was also found to be related to abnormally high associated with large winds. Thus, the observations that dropped in the time window 0.4–0.8 h may have a higher chance to provide negative impacts on the predictions if there is an abnormally high systems associated with high near surface wind speeds. As shown in Fig. 3, when those two anomalous events are excluded, the bias and RMSE dropped about 0.1 when time window is larger than 0.8 h whereas impact on time window smaller than 0.8 h is relatively limited and the tendency of the curve remains almost the same.

Figure 5 plots the histogram of the differences between the observed and predicted wind directions at different forecast lead times. No significant difference in the distribution of wind directions was observed between the 0.01 and 3.0 h time window configurations at both 6 and 24 h forecast lead times. The results for the 3.0 h time window showed only a slightly higher (0.6 and 0.1%) difference in wind direction in the $0\text{--}20^\circ$ range than the 0.01 h time window results at forecast lead times of 6 and 24 h, respectively. Figure 2 shows that although the initial wind field was more clearly modified as the time window increased, the predictions were not significantly affected. The differences in predicting wind speed and wind direction are more related to the model dynamical processes. Wind directions are still under the influences of background wind fields at a horizontal resolution of 9 km. In contrast, boundary layer wind speed is more affected by the boundary layer model schemes. The imperfection of numerical models may lead to larger differences in wind speed predictions.

5. Conclusions

The performance of near-surface wind prediction in eastern China was studied for different time window configurations in the GSI 3D-Var scheme. A series of numerical experiments with time windows varying from 0.01 to 3.0 h were conducted in the winter of 2017–2018. The statistical results were analyzed to explore the relations between the prediction of near-surface winds and the configuration of the time window.

The results were very different from our expectations, which were that better prediction would be obtained for observations that were closer in times. However, we found that the relationships between the observational times and the model forecast were non-linear. The results with a closer observational time to the initial time of the model had a positive impact on the prediction of near-surface wind speed, but this was limited to the 0.4 h time window.

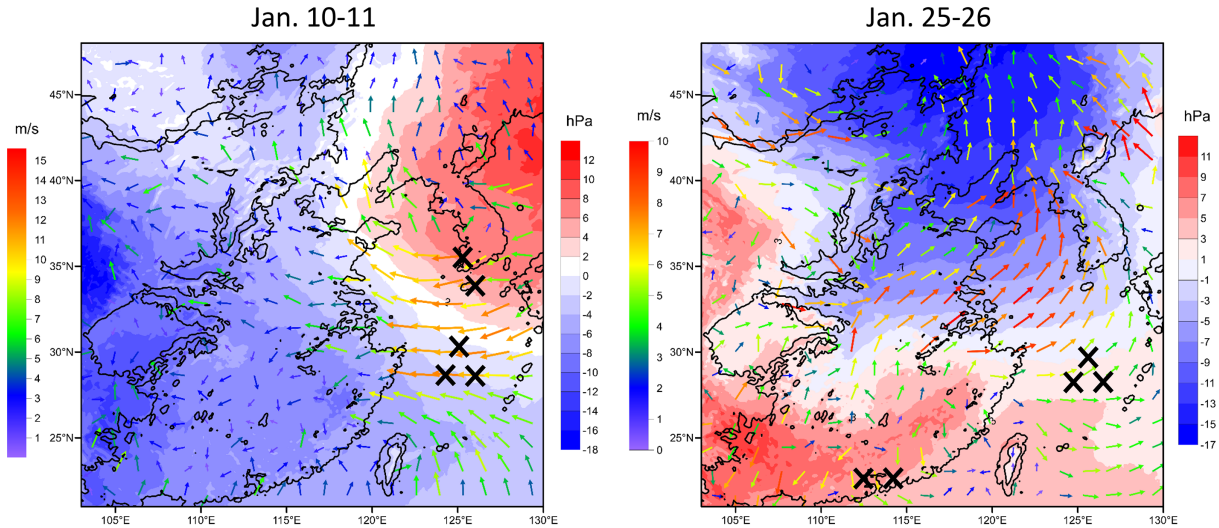


Fig. 4. SLP and 10 m height wind vector anomaly during the periods with large biases. Large biases regions are marked with “X”.

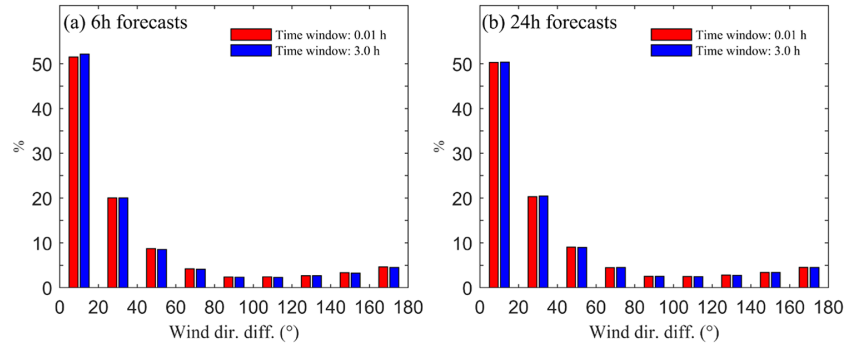


Fig. 5. Histogram of wind direction differences in (a) 6 h forecasts and (b) 24 h forecasts. The red bars indicate the results from time window for 0.01 h and the blue bars indicate the results from the time window for 3.0 h.

Observations in the 0.4–0.8 h time window could introduce more uncertainties especially when the observations are NEXRAD or an abnormally high system region associated with large near surface winds. The predictions improved again, although at a slower rate, when the time window was increased from 0.8 to 2.0 h. When the time window of observations in the GSI system were > 2.0 h, there was little difference in its effect on the prediction of near-surface winds. The optimum time window in the GSI 3D-Var system to minimize the forecast bias in the prediction of near-surface wind speeds is therefore 0.2 or 0.4 h. In contrast with the wind speed predictions, the predictions of wind direction did not show a significant difference when the time window was increased, even if the near-surface increments showed large differences in wind direction.

Acknowledgments

This work was supported by the National Key R&D Program of China (2016YFC0208504) and the Scientific Research Project of Tianjin Meteorological Bureau (201761bsjj06). The GSI DA system was obtained from the Joint Center for Satellite Data Assimilation, the WRF-ARW model was obtained from the National Center for Atmospheric Research and the satellite datasets were provided by the National Oceanic and Atmospheric Administration/National Environmental Satellite, Data, and Information Service/Center for Satellite Applications and Research. The authors thank these agencies for provision of the model and data.

Edited by: S.-H. Chen

References

- Anderson, E., and H. Jarvinen, 1998: Variational Quality Control. *Quart. J. Roy. Meteor. Soc.*, **125**, 697–722.
- Baker, N. L., T. F. Hogan, W. F. Campbell, R. L. Pauley, and S. D. Swadley, 2005: The impact of AMSU-A radiance assimilation in the U. S. Navy’s Operational Global Atmospheric Prediction System (NOGAPS). Marine Meteorology Division, Naval Research Laboratory, Memo. NRL/MR/7530-05-8836, 22 pp.
- Belusic, D., and I. Guttler, 2010: Can mesoscale models reproduce meandering motions? *Quart. J. Roy. Meteor. Soc.*, **136**, 553–565.
- Benjamin, S. G., G. A. Grell, J. M. Brown, and T. G. Smirnova, 2004: Mesoscale weather prediction with the RUC hybrid isentropic-terrain-following coordinate model. *Mon. Wea. Rev.*, **132**, 473–494.
- Benjamin, S. G., S. S. Weygandt, J. M. Brown, and co-authors, 2016: A north American hourly assimilation and model forecast cycle: The rapid refresh. *Mon. Wea. Rev.*, **144**, 1669–1694.
- Chavas, D. R., R. C. Izaurralde, A. M. Thompson, and X. J. Gao, 2009: Long-term climate changes impacts on agricultural productivity in eastern China. *Agri. Forest Meteor.*, **149**, 1118–1128.
- Chen, P. L., T. J. Wang, X. Hu, and M. Xie, 2015: Chemical mass

- balance source apportionment of size-fractionated particulate matter in Nanjing, China. *Aerosol Air Qual. Res.*, **15**, 1855–1867.
- Courtier, P., E. Andersson, W. Heckley, J. Pailleux, D. Vasiljevic, M. Hamrud, A. Hollingsworth, F. Rabier, and M. Fisher, 1998: The ECMWF implementation of three-dimensional variational assimilation (3D-Var). I: Formulation. *Quart. J. Roy. Meteor. Soc.*, **124**, 1783–1807.
- Cucurull, L., and R. A. Anthes, 2014: Impact of infrared, microwave, and radio occultation satellite observations on operational numerical weather prediction. *Mon. Wea. Rev.*, **142**, 4164–4186.
- Grell, G. A., and S. R. Freitas, 2014: A scale and aerosol aware stochastic convective parameterization for weather and air quality modeling. *Atmos. Chem. Phys.*, **14**, 5233–5250.
- Hu, M., H. Shao, D. Stark, K. Newman, C. Zhou, and X. Zhang, 2016: *Grid-point Statistical Interpolation (GSI) User's Guide Version 3.5*. Developmental Testbed Center, 141 pp (Available online at <http://www.dtcenter.org/com-GSI/users/docs/index.php>, accessed 1 April 2019).
- Iacono, M. J., J. S. Delamere, E. J. Mlawer, M. W. Shephard, S. A. Clough, and W. D. Collins, 2008: Radiative forcing by longlived greenhouse gases: Calculations with the AER radiative transfer models. *J. Geophys. Res.*, **113**, D13103.
- James, E. P., and S. G. Benjamin, 2017: Observation system experiments with the hourly updating rapid refresh model using GSI hybrid ensemble-Variational data assimilation. *Mon. Wea. Rev.*, **145**, 2897–2918.
- Kalnay, E., 2003: *Atmospheric Modeling, Data Assimilation and Predictability*, Cambridge University Press, 115 pp.
- Kleist, D. T., D. F. Parrish, J. C. Derber, R. Treadon, W. S. Wu, and S. Lord, 2009: Introduction of the GSI into the NCEP Global Data Assimilation System. *Wea. Forecasting*, **24**, 1691–1705.
- Lorenc, A. C., 2003: The potential of the ensemble Kalman filter for NWP – a comparison with 4D-Var. *Quart. J. Roy. Meteor. Soc.*, **129**, 3183–3203.
- Mahrt, L., 2011: Surface wind direction variability. *J. Appl. Meteor. Climatol.*, **50**, 144–152.
- Nakanishi, M., and H. Niino, 2009: Development of an improved turbulence closure model for the atmospheric boundary layer. *J. Meteor. Soc. Japan*, **87**, 895–912.
- Rabier, F., A. McNally, E. Andersson, P. Courtier, P. Uden, J. Eyre, A. Hollingsworth, and F. Bouttier, 1998: The ECMWF implementation of three-dimensional variational assimilation (3D-Var). II: Structure function. *Quart. J. Roy. Meteor. Soc.*, **124**, 1809–1829.
- Skamarock, W. C., J. B. Klemp, J. Dudhia, D. O. Gill, D. M. Barker, M. G. Duda, X. Y. Huang, W. Wang, and J. G. Powers, 2008: *A description of the Advanced Research WRF version 3*. NCAR Tech. Note NCAR/TN-475+STR, 124 pp.
- Stauffer, D. R., and N. L. Seaman, 1991: Use of four-dimensional data assimilation in a limited-area mesoscale model, Part 2: Effect of data assimilation within the planetary boundary layer. *Mon. Wea. Rev.*, **119**, 734–754.
- Thompson, G., P. R. Field, R. M. Rasmussen, and W. D. Hall, 2008: Explicit forecasts of winter precipitation using an improved bulk microphysics scheme. Part II: Implementation of a new snow parameterization. *Mon. Wea. Rev.*, **136**, 5095–5115.
- Wang, W., and co-authors, 2011: *ARW Version 3 Modeling System User's Guide*. Mesoscale and Microscale Meteorology Division, National Center for Atmospheric Research, 361 pp.
- Xu, J., S. Rugg, M. Horner, and L. Byerle, 2009: Application of ATVOS Radiance with ARW WRF/GSI Data Assimilation System in the Prediction of Hurricane Katrina. *Open Atmos. Sci. J.*, **3**, 13–28.
- Yang, J. B., H. N. Liu, and J. N. Sun, 2018: Evaluation and application of an online coupled modeling system to assess the interaction between urban vegetation and air quality. *Aerosol Air Qual. Res.*, **18**, 693–710.
- Zapotocny, T. H., J. A. Jung, J. F. Le Marshall, and R. E. Treadon, 2008: A two-season impact study of four satellite data types and rawinsonde data in the NCEP global data assimilation system. *Wea. Forecasting*, **23**, 80–100.
- Zhang, D. Q., and W. L., Song, 2018: Northern hemisphere atmospheric circulation characteristics in 2017/2018 winter and its impact on weather and climate in China. *Meteor. Mon.*, **44**, 969–976.
- Zhang, F. M., and C. H. Wang, 2014: Experiment of surface-layer wind forecast improvement by assimilating conventional data with WRF-3DVAR. *Plateau Meteor.*, **33**, 675–685.
- Zhang, F. M., Y. Yang, and C. H. Wang, 2015: The effects of assimilating conventional and ATVOS data on forecasted near-surface wind with WRF-3DVAR. *Mon. Wea. Rev.*, **143**, 153–164.
- Zou, J., G. Liu, J. N. Sun, H. S. Zhang, and R. M. Yuan, 2015: The momentum flux-gradient relations derived from field measurements in the urban roughness sublayer in three cities in China. *J. Geophys. Res. Atmos.*, **120**, 10797–10809.

*Manuscript received 1 April 2019, accepted 4 July 2019
SOLA: <https://www.jstage.jst.go.jp/browse/sola/>*